Multi-split type Gas-Engine-Driven Heat pump System Model to Estimate Performance in Low Temperature and High Humidity Conditions in Mid-winter

Eisuke Togashi
Kogakuin University, Tokyo, Japan

Introduction

A gas-engine-driven heat pump (GEHP) shows higher thermal capability than an electric heat pump (EHP) in winter because it uses residual heat from the engine exhaust. A GEHP rarely needs defrosting, which otherwise significantly reduces the efficiency of a heat pump system. The widespread use of multi-split type heat pump systems in commercial buildings has helped in enabling individual zone control. To evaluate the characteristics of a multi-split type GEHP, heat recovery from a gas engine, defrosting in an evaporator, and heat flow between indoor and outdoor units should be expressed quantitatively.

Elgendy et al. (2011) developed a semiempirical GEHP model that consists of a scroll compressor and plate evaporator. However, they did not address heating operations. Zhang et al. (2005) and Zhang et al. (2014) developed a GEHP model for the heating mode. However, these models are not multi-split type, and hence, cannot be applied to individual zone control systems. Hornberger developed a TRNSYS subroutine, which simulates a GEHP. Physical formulas are used to evaluate evaporators and condensers in this model, and the compressors effectiveness is calculated from the pressure ratio. Unfortunately, the heat transfer coefficients of heat exchangers are fixed, and therefore, the defrosting phenomena cannot be simulated.

This study develops a multi-split type GEHP model that consists of a compressor, an indoor unit, and an outdoor unit. The model components are expressed with physical formulas to simulate defrosting phenomena in winter. Firstly, a simulation model of a frosting coil (outdoor unit) is described, and then sensitivity analysis is performed. Description of model for indoor units is skipped since they have no defrosting phenomena and are much simpler than outdoor unit models. Secondly, a GEHP simulation model and parameter estimation method for the model is described. Finally, the model is integrated with a building heat-load simulation model.

The simulation model of a frosting coil

General description of the model

Figure 1 shows the state change of moist air in a frosting coil. We assume that the air maintains constant relative humidity during cooling process. Vapors condense into droplets when the air is cooled below the dew point. The droplet water freezes when the air temperature falls below the freezing point. As shown in figure 1, there exist two kinds of freezing processes. The upper diagram occurs when the absolute humidity of the inlet air is higher than that at freezing point. In this case, the coil is separated into three sections, dry, wet, and frosting part. The lower diagram occurs when the absolute humidity of the inlet air is lower than that at freezing point. In this case, the coil has no wet part. In this paper, the subscripts "d," "w," "f," "wb," and "fb" represents dry coil, wet coil, frosting coil, wet border, and frost border, respectively. Heat transfer of the evaporator Q_{evp} [kW] can be calculated by integrating the heat transfers in each part, as shown in equation (1).
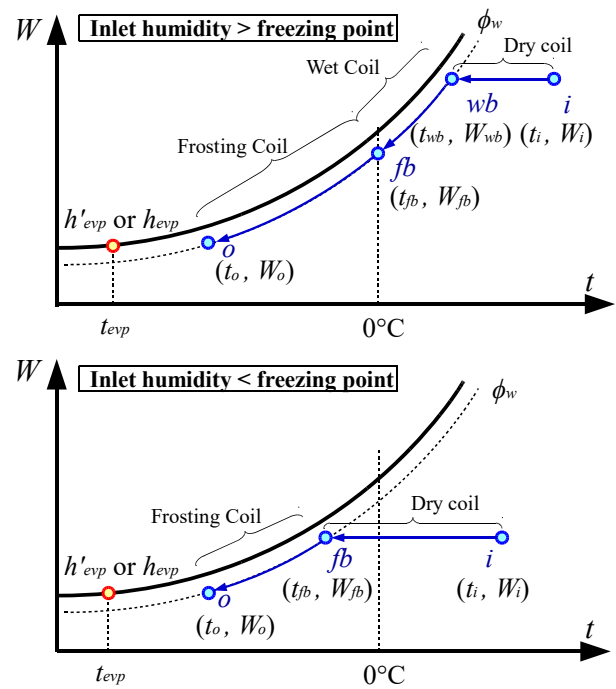

Figure 1: State change of moist air in a frosting coil

$$Q_{evp} = Q_d + Q_w + Q_f \qquad (1)$$

Basic formulae used in the model

Heat transfer in the dry coil is given by the equations (2) and (3). It is calculated from inlet temperature (t_i [°C]) and outlet temperature (t_{wb} [°C]) difference of moist air as shown in the equation (2), where mc_a [kW/K] is the heat capacity rate of the moist air. Heat transfer can be also modeled with effectiveness (ε_d [-]), as shown in the

equation (3). t_{evp} [°C] is the evaporating temperature, which can be assumed as constant value during the cooling process. If one fluid remains at a constant temperature throughout the heat exchange, effectiveness can be calculated from equation (4), where K_d [kW/(m²·K)] and S_d [m²] are heat transfer coefficient and surface area of the coil, respectively. K_d is calculated from air face velocity v_a [m/s], as shown in equation (5), where v_{sa} [m/s] is the reference air face velocity (= 2.0 m/s). The coefficients used in equation (5) are estimated from Inoue's research (2008) with regression analysis. Since air face velocity is usually designed in the range of 1.5~2.5 m/s and the density changes of moist air is very small, equation (6) is used in this model instead of equation (5). m_a [kg/s] and m_{aN} [kg/s] are mass flow rates of moist air at operating and nominal conditions, respectively.

$$Q_d = mc_a(t_i - t_{wb}) \tag{2}$$

$$Q_d = \varepsilon_d mc_a(t_i - t_{evp}) \tag{3}$$

$$\varepsilon_d = 1 - \exp(-K_d S_d / mc_a) \tag{4}$$

$$K_d = 0.0236(v_a/v_{sa})^{0.5479} \tag{5}$$

$$K_d = 0.0236(m_a/m_{aN})^{0.5479} \tag{6}$$

Heat transfer in the wet coil is given by the equation (7) and (8). It is calculated from inlet specific enthalpy (h_{wb} [kJ/kg]) and outlet specific enthalpy (h_{fb} [kJ/kg]) difference of moist air. as shown in the equation (7). The equation (8) is an effectiveness model, where $h_{S,evp}$ [kJ/kg] is the specific enthalpy of saturated moist air at the evaporating temperature, t_{evp}. Specific enthalpy $h_{S,evp}$ is calculated from the equation (10). c_{pa}, γ_{v0}, c_{pv}, and $W_{S,evp}$ represent the isobaric specific heat of dry air (1.006 kJ/(kg·K)), water vaporization heat at 0 °C (2,501 kJ/kg), isobaric specific heat of vapor (1.805 kJ/(kg·K)), and saturated absolute humidity at the evaporating temperature (t_{evp}), respectively. Effectiveness ε_w, can be calculated from the equation (9), where K_w [kW/(m²·(kJ/kg))] and S_w [m²] are heat transfer coefficient and surface area of the wet coil, respectively. From the analogy between heat and mass transfers, K_w can be calculated from the equation (11). Because the value of isobaric specific heat of the moist air c_{pma} [kJ/(kg·K)] alters during the cooling process, the model uses the average of specific heat at wet border and frost border, as shown in the equation (12).

$$Q_w = m_a(h_{wb} - h_{fb}) \tag{7}$$

$$Q_w = \varepsilon_w m_a(h_{wb} - h_{S,evp}) \tag{8}$$

$$\varepsilon_w = 1 - \exp(-K_{wf} S_w / m_a) \tag{9}$$

$$h_{S,evp} = c_{pa}t_{evp}(\gamma_{v0} - c_{pv}t_{evp})W_{S,evp} \tag{10}$$

$$K_w = K_d/(c_{pa} + c_{pv}W) = K_d/c_{pma} \tag{11}$$

$$c_{pma,w} = 0.5(c_{pma,wb} + c_{pma,fb}) \tag{12}$$

Heat transfer in the frosting coil is almost same as that in the wet coil. The specific heat h' [kJ/kg] is redefined, as shown in the equation (16). The equation takes solid

state as the reference state, where γ_{s0} and s_{ps} are the water sublimation heat at 0 °C (2,837 kJ/kg) and isobaric specific heat of ice (2.09 kJ/(kg·K)). Since the heat transfer coefficient decreases when frost occurs, the collection factor C_{ff} [-] is introduced, as shown in the equation (15). Aoki (1986) developed a detailed model to estimate the heat transfer coefficient of the frosting coil. From Aoki's result, the collection factor C_{ff} takes values between 0.5~0.6 when the thickness of frost is 1 mm and the air face velocity is 5~15 m/s. As C_{ff} tends to take large values when the velocity is low, C_{ff} is fixed to 0.6 in the model developed in this research. To calculate the heat transfer coefficient K_w in the frosting coil, the specific heat at frost border $c_{pma,fb}$ is used instead of c_{pma} in the equation (11). Since the coil must warm up to 0 ºC to take off the frost by melting, defrosting heat Q_{df} [kW] is expressed by the equation (18).

$$Q_f = m_a(h'_{fb} - h'_o) \tag{13}$$

$$Q_f = \varepsilon_f m_a(h'_{fb} - h'_{S,evp}) \tag{14}$$

$$\varepsilon_f = 1 - \exp(-C_{ff}K_w S_f / m_a) \tag{15}$$

$$h' = c_{pa}t(\gamma_{s0} - c_{ps}t)W \tag{16}$$

$$h'_{S,evp} = c_{pa}t_{evp}(\gamma_{s0} - c_{ps}t_{evp})W_{S,evp} \tag{17}$$

$$Q_{df} = m_a(\gamma_{s0} - c_{ps}t_o)(W_{fb} - W_o) \tag{18}$$

Solution algorithm

To simulate refrigerant cycles, three solution algorithms are required. The first algorithm is the estimation of surface area S [m²] from nominal conditions. The second is the estimation of heat transfer Q_{evp} from the evaporating temperature t_{evp}. The third is the estimation of evaporating temperature t_{evp} from the heat transfer Q_{evp}.

Figure 2 shows the flow diagram of surface area estimation from nominal conditions (evaporative temperature, heat transfer, moist air state, and airflow rate).
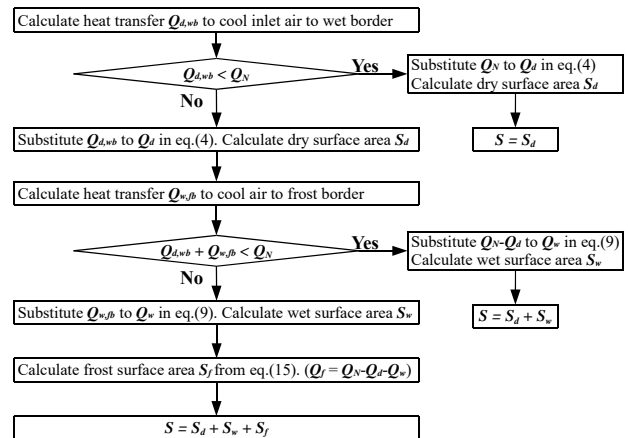

Figure 2: Flow diagram of surface area estimation

First, we calculate the heat transfer Q_d to cool the moist air down to the wet border. If Q_d is bigger than the nominal heat transfer Q_N [kW], there are no wet coil sections, and dry surface area S_d equals the surface area

S. In this case, we calculate surface area S_d from the equations (3) and (4), substituting Q_N for Q_d.

If Q_d is smaller than Q_N, heat transfer at the wet coil should be solved. Calculate heat transfer Q_w to cool down the moist air from wet border to frost border. If the summation of Q_d and Q_w is greater than Q_N, there are no frost coil sections. In this case, the summation of S_d and S_w is equal to S.

If the summation of Q_d and Q_w is smaller than Q_N, calculate the frost-coil surface area S_f from the equation (15) and summate each surface area.

Figure 3 shows the flow diagram of heat transfer estimation from evaporating temperature.
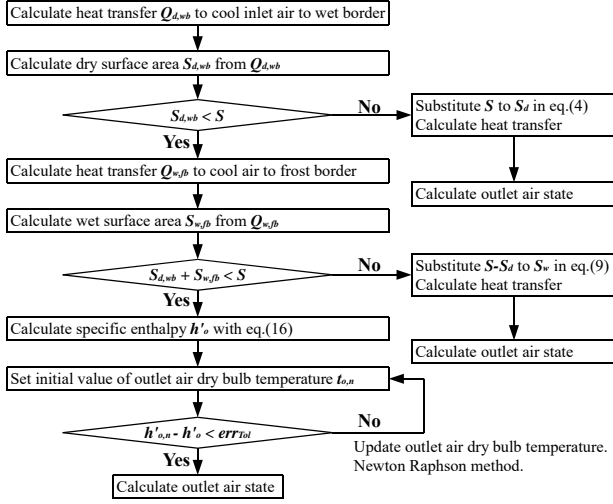

Figure 3: Flow diagram of heat transfer estimation

First, we calculate dry surface area S_d to cool the moist air down to the wet border. If S_d is greater than the surface area S, heat transfer is completed before the moist air reaches the wet border. In this case, calculate heat transfer Q_d ($=Q$) from the equation (3) and (4) by substituting S for S_d.

If S_d is smaller than surface area S, dehumidification at the wet coil has started. Calculate the wet surface area S_w to cool down the moist air from the wet border to the frost border. If the summation of S_d and S_w is greater than S, there are no frost coil sections; else, frost has occurred and the outlet moist air state is calculated iteratively in this case.

To calculate evaporating temperature from heat transfer, we make an error function and use iterative method. The inputs of the error function are the heat transfer and initial guess of the evaporating temperature. The output (error) of the error function is the difference between the heat transfer, which is calculated from the assumed evaporating temperature using the algorithm shown in Figure 3, and the input value. Nonlinear solving methods such as the Newton Raphson method can be used to solve this error function.

Sensitivity analysis

Sensitivity analysis is performed to examine the accuracy of the model. Table 1 shows the nominal specifications of the evaporator to be simulated.

Table 1: Nominal specification of the evaporator

Evaporating temperature	2 ºC
Inlet air dry bulb temperature	7 ºC
Inlet air wet bulb temperature	6 ºC
Volumetric air flow rate	167 m³/h
Heat transfer	13 kW
Relative humidity at wet border	95 %

Figure 4 shows the result of the sensitivity analysis. The left side diagrams show the relation between inlet dry bulb temperature and heat transfer; the right side diagrams show the relation between inlet dry bulb temperature and defrosting load. The lines are drawn by different evaporating temperatures in the upper diagrams (relative humidity=85% const.), and by different relative humidity in the lower diagrams (evaporating temperature = 2 ºC const.). Heat transfer increases at lower evaporating temperatures. Defrosting load shows local maximum around 1 ∼ 2 ºC. When the dry bulb temperature is high, the heat transfer increases at higher relative humidity since the rate of latent heat exchange is large. When the dry bulb temperature is low, the effect of relative humidity becomes lower, since the rate of sensible heat exchange becomes large.
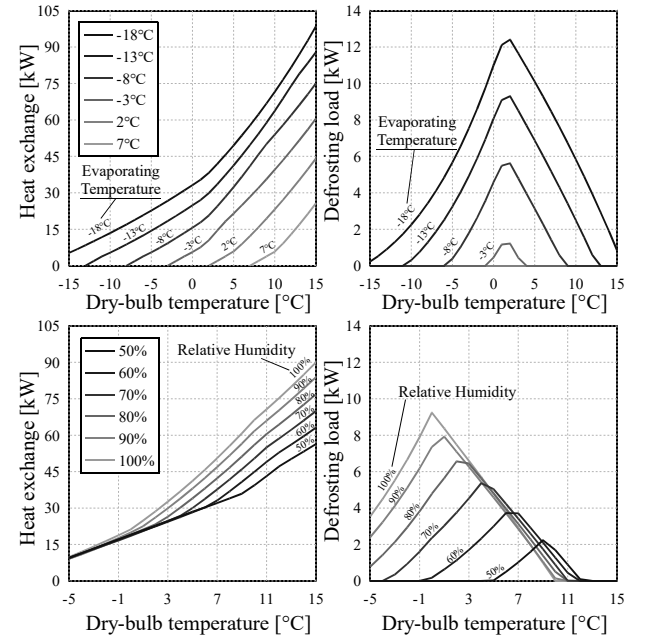

Figure 4: Result of the sensitivity analysis (Evaporator)

The simulation model of a GEHP

General description of the model

Figure 5 shows the energy flow diagram of the model. Key points of this model are the treatment of heat recovered from the gas engine exhaust and defrosting load. Q_{rcv} [kW] is recovered by the heat exchanger and transferred into the inlet refrigerant at the compressor. When the evaporator develops frost, hot gas refrigerant is bypassed and Q_{df} is supplied from the compressor. Q_{rcv} increases, while Q_{df} decreases the heat supply Q_{cnd} [kW] to the condenser, which affects the efficiency of heat

pump system. The defrosting load is calculated with the theoretical model of the evaporator described above.
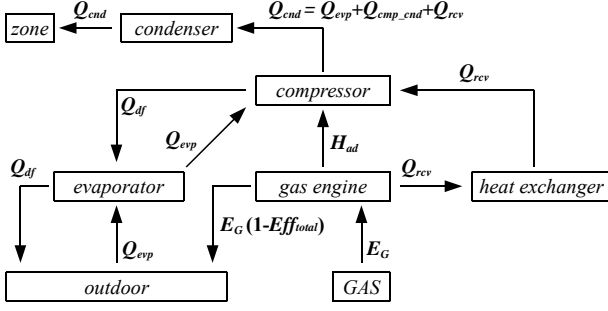

Figure 5: Energy flow diagram of the model

Basic formulae used in the model

The equations (19) ~ (28) are the basic formulae used in this model. The head of the compressor H_{ad} [kW] is obtained by multiplying collection factor C_{fG} [-], gas consumption E_G [kW], and head efficiency Eff_{had} [-], as shown in the equation (19). Compression efficiency Eff_{had} is expressed as a function (the specific formula will be described later) of partial load pl [-]. Partial load pl can be calculated with the equation (20), where $H_{ad,N}$ [kW] is the nominal head of the compressor. The head of the compressor can be also calculated from the condensing pressure P_{cnd} [kPa], evaporating pressure P_{evp} [kW], refrigerant flow rate vf_R [m³/s] and ratio of specific heat κ [-], as shown in the equation (21).

When the coil has frosted, part of the head is lost to defrost energy Q_{df} [kW]; rest of the head Q_{cmp_cnd} [kW] is supplied to indoor units. The total efficiency of the gas engine Eff_{ttl} [-] is broken down into heat recovery efficiency Eff_{rcv} [-] and head efficiency Eff_{had}, as shown in the equation (23). Since the total efficiency Eff_{ttl} is assumed to be constant in this model, heat recovery efficiency Eff_{rcv} can be calculated from the head and gas consumption, as shown in the equation (24). Recovery heat is calculated by multiplying the heat recovery efficiency and gas consumption (eq. 25).

Heat load at the evaporator Q_{evp} is calculated by subtracting the head and recovery heat from the heat load at the condenser Q_{cnd}. Q_{cnd} is the summation of indoor unit loads as shown in the equation (27), where C_{fp} [-] is the collection factor, which depends on the pipe length of indoor unit. The volumetric flow rate of refrigerant vf_R [m³/s] is expressed by the equation (28), where ρ_{evp} [kg/m³] and h_{evp} [kJ/kg] is the density and enthalpy of the refrigerant at the evaporator, respectively.

$$H_{ad} = C_{fG} \cdot E_G \cdot Eff_{had} = C_{fG} \cdot E_G \cdot f(pl) \quad (19)$$

$$pl = H_{ad}/H_{ad,N} \quad (20)$$

$$H_{ad} = \frac{\kappa}{\kappa - 1} P_{evp} vf_R \left\{ \left(\frac{P_{cnd}}{P_{evp}} \right)^{\frac{\kappa-1}{\kappa}} - 1 \right\} \quad (21)$$

$$H_{ad} = Q_{cmp\_cnd} + Q_{df} \quad (22)$$

$$Eff_{ttl} = Eff_{rcv} + Eff_{had} \quad (23)$$

$$Eff_{rcv} = Eff_{ttl} - H_{ad}/E_G \quad (24)$$

$$Q_{rcv} = Eff_{rcv} \cdot E_G \quad (25)$$

$$Q_{evp} = Q_{cnd} - H_{ad} - Q_{rcv} \quad (26)$$

$$Q_{cnd} = \sum_{n=0}^{N} \frac{Q_{cnd,n}}{C_{fp}} \quad (27)$$

$$vf_R = \frac{Q_{evp} + Q_{rcv}}{\rho_{evp,o}(h_{evp,o} - h_{evp,i})} \quad (28)$$

Solution algorithm

Figure 6 shows the refrigeration cycle of the model. In this model, outlet refrigerant states of the evaporator and condenser are assumed to be saturated vapor and liquid, respectively. The upper limit of the evaporating temperature and the lower limit of the condensing temperature is set to 10 ºC and 40 ºC, respectively.
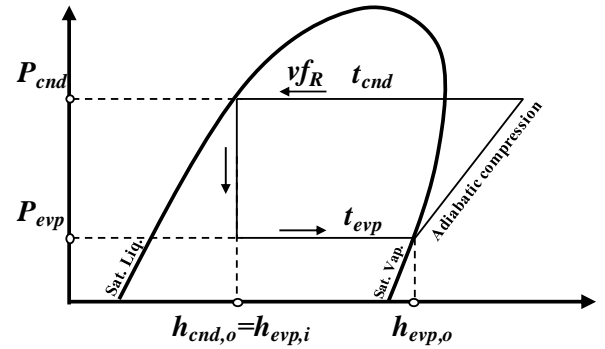

Figure 6: Refrigeration cycle of the model

Figure 7 shows the flow diagram of the GEHP model. Firstly, we calculate the heat load $Q_{cnd,n}$ and condensing temperature $T_{cnd,n}$ [kW] of each indoor unit. The condensing pressure $P_{cnd,max}$ [kPa] of the GEHP is determined by the highest condensing temperature of the indoor unit.

Next, we calculate the minimum heat transfer $Q_{evp,min}$ [kW] at the evaporator by substituting max head $H_{ad,max}$ [kW] for H_{ad} in the equation (26). Using the evaporator model described above, the evaporating temperature can be calculated from heat transfer $Q_{evp,min}$. The pressure P_{evp}, specific enthalpy $h_{evp,o}$, heat capacity rate κ and density $\rho_{evp,o}$ of saturated vapor can be estimated from saturated temperature (=evaporating temperature) with the thermodynamic calculation method of refrigerant (Togashi (2014)). The volumetric refrigerant flow rate vf_R can be calculated by substituting $\rho_{evp,o}$ and $h_{evp,o}$ in the equation (28). We calculate head $H^*_{ad,max}$ by substituting these value in the equation (21).

If $H^*_{ad,max}$ is greater than the assumed max head $H_{ad,max}$, the GEHP system cannot solve the heat load. In this case, we fix H_{ad} to the maximum value ($H_{ad,max}$), then estimate condensing pressure P_{cnd} with iterative calculation. The solution of P_{cnd} exists between 0 to $P_{cnd,max}$. If $H^*_{ad,max}$ is smaller than the assumed max head $H_{ad,max}$, the GEHP system can solve heat load. In this case, fix P_{cnd} to $P_{cnd,max}$, then estimate the head H_{ad} with iterative calculation. The solution of H_{ad} exists between 0 to $H_{ad,max}$.

Since GEHP shows nonlinear characteristics when defrost occurs, the Newton Raphson method sometimes fails. The Golden section method, Bisection method or Brent method are preferred for this iterative calculation.
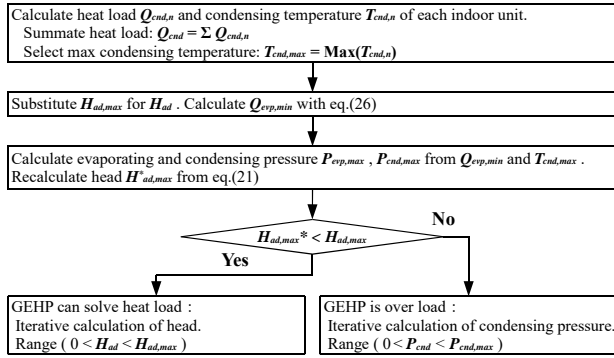

Figure 7: Flow diagram of the GEHP model

Parameters estimation

The total efficiency Eff_{ttl}, head efficiency Eff_{had} and airflow rate of indoor and outdoor units are estimated from the manufacturers' data sheets.

The GEHP does not use outdoor air as a heat source when outdoor air temperature is very low. In this case, the total efficiency Eff_{ttl} can be calculated by dividing the heating capacity Q_{cnd} by the gas consumption, because the heating capacity Q_{cnd} equals summation of the head H_{ad} and heat recovery Q_{rcv}. From the data sheets of manufacturer A, in the case of outdoor air temperature is -20 ºC, the total efficiency Eff_{ttl} is estimated to exist between 78.2 ~ 86.8%. In this model, 80% is used for total efficiency Eff_{ttl}.

Figure 8 shows relation between partial load and head efficiency. The data is estimated from the data sheet of 45 kW GEHP supplied by the manufacturer A. The evaporating and condensing temperature at nominal condition is assumed to be 2 ºC and 50 ºC, respectively, to initialize the surface area of the evaporator and condenser. The data at defrosting condition is removed to eliminate influence of hot gas bypass control.
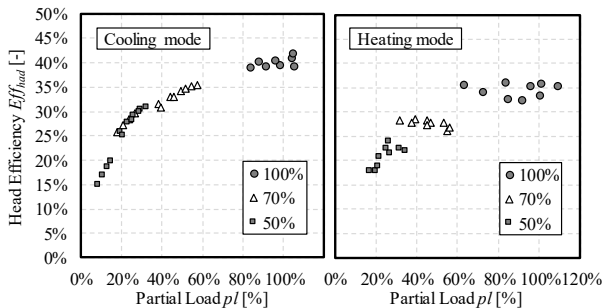

Figure 8: Relation of partial load and head efficiency-1

It is inconvenient to use different head efficiency characteristic curves for different operating modes or different capacities, hence, a general characteristic curve should be made. Figure 9 is characteristic curve made from 45 kw, 56 kW and 71 kW GEHP in heating and cooling modes. In this model, we use the same characteristic curve. Collection factor C_{fG} in equation

(19) is used to adjust gas consumption at nominal conditions (100% load) to gas consumption calculated from this curve. If the partial load is lower than 5%, it is treated as 5%.
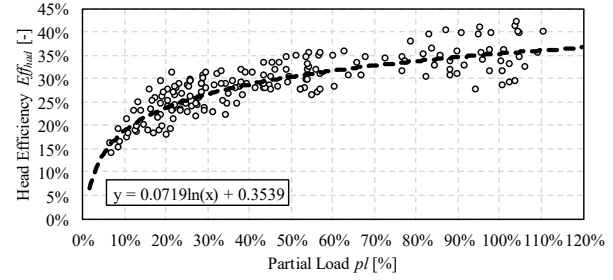

Figure 9: Relation of partial load and head efficiency-2

Figures 10 and 11 show relation between the cooling capacity and airflow rate of indoor and outdoor units. The figure are made by 3 manufactures' 5 type units. It is seen that the airflow rate of different type indoor units can be expressed with a single approximation formula. In this model, the airflow rates of the units are initialized using cooling capacity with this formula.
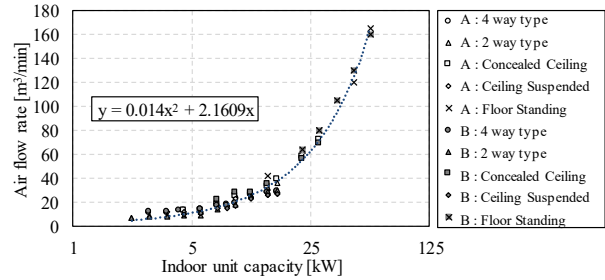

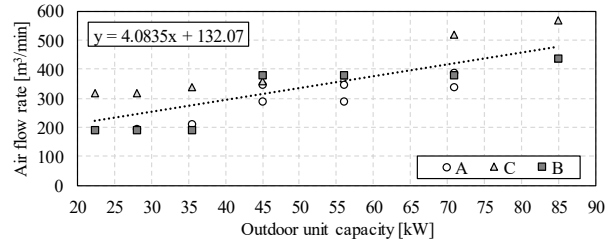*Figure 10: Relation between indoor unit cooling capacity and airflow rate*

Figure 11: Relation between outdoor unit cooling capacity and airflow rate

Sensitivity analysis

The GEHP, which has 10 indoor units was modeled to perform sensitivity analysis. The cooling capacity of outdoor and indoor units are 45 kW and 4.5 kW, respectively (heating capacity is 50 kW and 5.0 kW, respectively). Two operating cases are simulated. One case is that each indoor unit has the same heat load, and other is case that heat load of one indoor unit remains full load (100%). Figure 12 shows relation between the partial load rate and gas consumption or compression ratio. As the partial load rate increases, both gas consumption and compression ratio increase. If the loads of the indoor units decrease uniformly, the gas consumption decreases much faster than under the

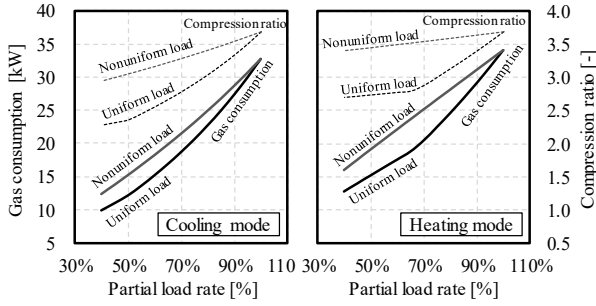influence of an imbalanced load, since the full load indoor unit requires a high condensing temperature.

Figure 12: Relation between partial load rate and gas consumption or compression ratio

Figure 13 shows the relations between the outdoor temperature and heating performance of the GEHP.

Two models, one with heat recovery and the other with no heat recovery, are simulated. The heat recovery efficient Eff_{rcv} is set to 0 in the model, which has no heat recovery. The surface area and outdoor unit's airflow rate of no heat recovery models are raised about 10% higher to make the heating capacity of both models same at nominal conditions.

Defrosting load occurs when the temperature becomes 4.5 ºC and 3.0 ºC, respectively, in no heat recovery case and heat recovery case. The relative humidity is fixed to 80% in this simulation. If heat recovery is not performed, the defrosting load increases under low temperatures and lowers the COP (Coefficient Of Performance). In the heat recovery case, the heating capacity is about 25% higher than that of no heat recovery case, under low outdoor temperature (2.5 ºC or lower) conditions.
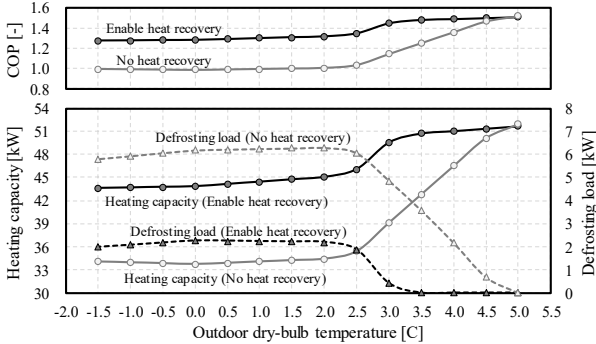

Figure 13: Relation between outdoor dry-bulb temperature and heating performance

Case study of mid-winter operation

The GEHP model was integrated with a building heat-load simulation model.

An office building located in Tokyo is simulated. Figure 14 shows the plan, section, elevation, and indoor units zoning of building. East side of floor is simulated. The number in the parenthesis in the Figure 14 is the peak cooling load. Since fresh air load is assumed to be solved by the outdoor air conditioning unit, the peak load of indoor units is the summation of indoor heat gains and skin load. Table 2 shows material specifications.

Figure 15 shows the heat gain schedule of the office. The vertical axis shows the ratio of load and peak load. The peak loads of lighting load, plug load, and occupancy are 10 W/m², 15 W/m² and 0.2 person/m², respectively. The sensible heat from the occupant is set to 94 W/person. This value is calculated from a two-node model under air condition of 22 ºC, 40%.

HVAC systems operate from 8:00 to 18:00 on weekdays (Office starting time is 9:00). Simulation is run from 11/1 to 3/31. The data from 12/1 to 3/31 is used in later discussions.

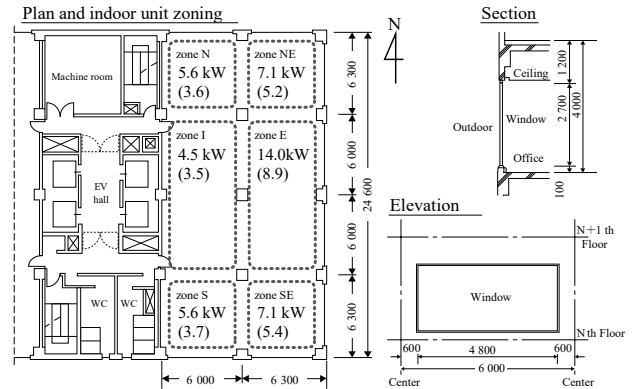The heat capacity of the room is 12 kJ/(m³·K) per room volume and air leakage is 0.4 times per hour.

Figure 14: Plan, section, elevation and indoor unit zoning of building

Table 2: Material specifications

|	
External wall	Rigid Urethane Foam 25 mm, Reinforced Concrete 150 mm, Mortar 20 mm, Tile 8 mm, Longwave Emissivity 0.9, Shortwave Emissivity 0.7
Indoor wall	Mortar 25 mm, Reinforced Concrete 150 mm, Mortar 25 mm
Floor	Carpet 6 mm, Reinforced Concrete 22 mm Air gap , Reinforced Concrete 150 mm, Air gap, Plaster Board 9 mm, Rock Wool Acoustic Board 12 mm
Window	Low emissivity double grazing glass. 8 mm glass, 6 mm air gap, 8 mm glass. Grey colored blind. (Pull downed when solar irradiance is larger than 100 W/m²)
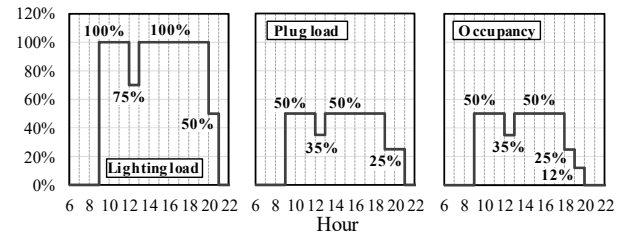
Figure 15: Heat gain schedule of office

Figure 16 shows the monthly heating load calculated by the model. To validate accuracy of the model by comparing simulation results with statistical measured values, fresh air load is included in this case. Versions of Expanded AMeDAS Reference Weather Year Data (EA-RWY) of the year 2000 are used for weather data. The annual heating load per office floor area is 81.2

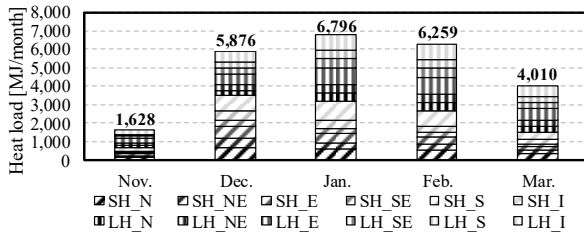MJ/(m^2·yr). This is the typical level for office buildings in Tokyo.

Figure 16: Monthly heating load

Simulation on winter season is performed with weather data measured in 1984, which is known as the hard winter year. Figure 17 shows the trend of temperature and COP on January 19th, which was the most cold and humid day in 1984. The upper chart shows the outdoor conditions. The risk of defrost operation is quite high on this day, because the dry bulb temperature is below freezing throughout the day, where absolute humidity maintained is 3.0~3.5 g/kg high. In case the GEHP has no heat recovery, defrost operation continues all day. If heat recovery is performed, the GEHP comes back to normal operation at 8:48. The room temperature reaches to a set point temperature at 8:58 and 10:37 in each case. It takes an hour and a half longer to warm up room temperature if there is no heat recovery. The daily averaged COP of GEHP is 1.19 and 0.77 on this day and the seasonal averaged COP of GEHP is 1.32 and 1.26 in this winter.
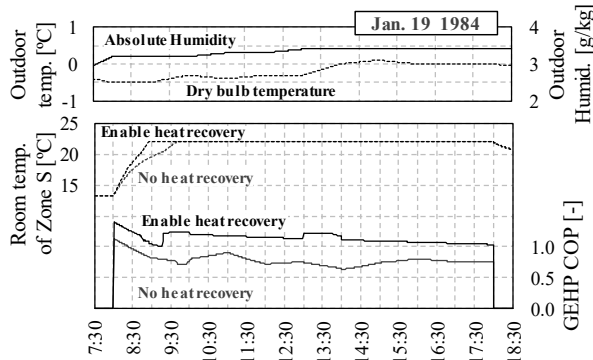

Figure 17: Trend of temperature and COP on low temperature and high humidity day in winter

Conclusion

This study develops a multi-split type GEHP model, which consists of a compressor, indoor units, and an outdoor unit. The model components are expressed with physical formulas to simulate defrosting phenomena in winter. The simulation model of a frosting coil is developed, and sensitivity analysis is performed. The simulation model of GEHP is developed, and the parameter estimation method for the model is described. Finally, daily and seasonal COP of GEHP is evaluated by integrating the GEHP model with the building heat-load simulation model.

Nomenclature

c_p	: Isobaric specific heat	[kJ/(kg·K)]
C_f	: Collection factor	[-]
err	: Error	
E_G	: Gas consumption	[kW]
h	: Specific enthalpy	[kJ/(kg·K)]
H_{ad}	: Head	[kW]
K	: Heat transfer coefficient	[kW/(m^2·K)]
m	: Mass flow rate	[kg/s]
mc	: Heat capacity rate	[kW/K]
n	: Number of iteration	[-]
n	: Number of indoor units	[-]
pl	: Partial load rate	[-]
P	: Pressure	[kPa]
Q	: Heat flow	[kW]
S	: Surface area	[m^2]
t	: Temperature	[°C]
v_a	: Face velocity of coil	[m/s]
vf	: Volumetric flow rate	[m^3/s]
W	: Absolute humidity	[kg/kg]
ε	: Effectiveness	[-]
κ	: Ratio of specific heat	[-]
γ	: Sensible heat	[kJ/kg]
ρ	: Density	[kg/m^3]

sub scripts:

a	: air	N	: Nominal
cnd	: condenser	p	: pipe
d	: dry	rcv	: recover
df	: defrost	R	: Refrigerant
evp	: evaporator	s	: standard
f	: frost	s	: solid
fb	: frost border	S	: Saturated
G	: Gas	ttl	: total
had	: head	v	: vapor
i	: inlet	w	: wet
ma	: moist air	wb	: wet border

Acknowledgement

References

R.R. Zhang, X.S. Lu, S.Z. Li, W.S. Lin, A.Z. Gu (2005). Analysis on the heating performance of a gas engine driven air to water heat pump based on a steady-state model. *Energy Conversion and Management,* Vol. 46, pp. 1714–1730.

X. Zhang, Z. Yanga, X. Wua, X.-C. Su (2014). Evaluation method of gas engine-driven heat pump water heater under the working condition of summer. *Energy and Buildings,* Vol. 77, pp. 440–444.

E. Elgendy, J. Schmidt, A. Khalil, M. Fatouh (2011). Modelling and validation of a gas engine heat pump working with R410A for cooling applications. *Applied Energy,* Vol.88, Issue 12, pp. 4980–4988.

M. Hornberger, G-PUMP - Simulation software for gas engine heat pumps, http://trnsys.de/download/en/ts_type_371_beta_en.pdf (accessed 2015-07-31)

U. Inoue, Air conditioning Handbook, Maruzen Co., Ltd., 2008, Chapter 7, p. 296

Kazuo Aoki, Masaru Hattori and Takeshi Itoh, A Study of Extended Surface Heat Exchanger with Frosting : 1st Report, Overall Heat Transfer Characteristics, Bulletin of JSME, Vol. 29, No. 251, 1986, pp. 1499-1505

Eisuke Togashi, Development of Equation of State for the Thermodynamic Properties of HFC 32 (R32) for the Purpose of Annual Building Energy Simulation, Transactions of the Society of Heating, Air-Conditioning and Sanitary Engineers of Japan, Vol. 204, March, 2014, pp. 69-76